HORN-BASED CIRCULAR POLARIZED ANTENNA AR-RAY WITH A COMPACT FEEDING FOR KA-BAND MONOPULSE ANTENNA

Yong Li Ren, Jian Wang*, Da Cheng Hu, and Ning Zhang

School of Electronic Engineering, University of Electronic Science and Technology of China, Chengdu 611731, P. R. China

Abstract—A pyramidal horn monopulse array is proposed for working at Ka-band with circular polarization (CP) characteristic. The array is composed of 28 elements with a 28-way waveguide power divider network. The element has a pyramidal horn with a rectangular waveguide, which is placed downside the horn. There is a 45° inclined slot cut in the wide wall of the rectangular waveguide. The inclined slot can convert the excitation into two orthogonal modes with equal amplitude, and 90° out of phase is produced due to different propagation constants of the two modes in the pyramidal horn. Therefore, the antenna can achieve CP by using a compact structure without polarizer. This paper also provides procedure of the compact power divider network for synthesizing monopulse pattern. This monopulse array has excellent performance: The simulated and measured reflection coefficients of the sum port and difference port of the array are below -15 dB, the side lobe level of array less than -27 dB, and axial ratio < 3 dB in the mainlobe beamwidth. The simulated and measured results are in good agreement.

1. INTRODUCTION

Monopulse direction finding technique is one of the most accurate and rapid methods for locating a target electronically [1]. A simple monopulse system combines the information received by two channels: the sum (Σ) and the difference (Δ) channels, which produce broadside patterns with a broad peak and sharp null, and allow a system to obtain information about the position of a target.

Horn antenna is an attractive choice for circularly polarized element [2–4]. A typical circularly polarized horn antenna consists of three major components: a wave launcher, a polarizer and a beam shaper [5]. The wave launcher is generally used at lower frequencies. At higher frequencies, the wave launcher is sometimes omitted since the energy is already in the form of a guided wave, and can be directly applied to the polarizer. Depending on the type of antenna to be fed, the beam shaper can be implemented in many ways. The polarizer is the most important component to generate the CP. CP is usually generated by using waveguide polarizer, which takes several forms. For instance, metallic septum in square waveguides [6, 7] or circular waveguides [8, 9] have been reported, and waveguide polarizers have also been proposed by adding corrugations [10], dielectric slab [11], irises [12], grooves [13] or by using lossy magnetic material [14, 15]. However, these polarizers always have large dimensions or complicated physical structure.

A novel pyramidal horn array with a compact power divider network is proposed in this paper. The element has a pyramidal horn with a rectangular waveguide, which is placed downside the horn. There is a 45° inclined slot cut in the wide wall of the rectangular waveguide. The inclined slot can convert the excitation into two orthogonal modes with equal amplitude, and 90° out of phase is obtained due to different propagation constants of the two modes in the pyramidal horn. Therefore, the antenna can achieve CP by using a compact structure without polarizer. In addition, to provide output amplitudes and phases exactly as required by the antenna array, the procedure of compact waveguide power divider network is also presented in this paper. As a result, with the power divider network, the overall size of the array will decrease without any performance deterioration.

This monopulse array is restricted by its structure due to mechanical scanning limitations. The antenna will keep its performance in spite of vibration and shock interference. The antenna array working at Ka-Band has 0.01 fc relative bandwidth, and fc represents the center frequency. The reflection coefficient at the ports of the array is below -15 dB, side lobe level (SLL) below -27 dB, axial ratio of Right Hand CP (RHCP) below 3 dB in the beamwidth, level difference of Δ beam below 1 dB, and null depth of the Δ beam below -22 dB. These characteristics imply that the antenna array has excellent performance.

2. ELEMENT DESIGN

2.1. Design Concept of the Element

To realize an element which has good CP performance in a compact structure, a pyramidal horn antenna with a short-circuited end rectangular waveguide is proposed. The structure of the element is illustrated in Fig. 1. A pin near the input port of the rectangular waveguide is designed for optimum impedance match.
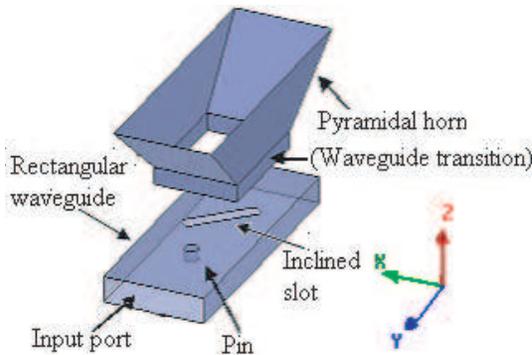
Figure 1. Structure of the pyramidal horn antenna.

There is a 45°-right inclined slot (from the top view in Fig. 2(a)) cut in the wide wall of the rectangular waveguide. The center of the inclined slot must coincide with the phase center of the pyramidal horn where the excitation takes place. By selecting the appropriate dimensions of the 45°-right inclined slot, the excitation in rectangular guide will be converted into two orthogonal modes (TE_{10} and TE_{10}) of equal amplitude. According to the waveguide mode theory, the field components in rectangular guide can be expressed in the normalized form [16]. And different modes have different propagation constants in a rectangular waveguide. The propagation constant β in the normalized form formula of the TE_{mn} modes can be expressed by

$$\beta = \sqrt{(2\pi/\lambda)^2 - (m\pi/a)^2 - (n\pi/b)^2} \qquad (1)$$

where a and b represent the length and weight of the port of rectangular waveguide respectively, and λ is the wavelength in the free space. In formula (2), selecting an appropriate length (l) of the waveguide will make different modes 90° out of phase:

$$\beta_1 l - \beta_2 l = \pi/2 \qquad (2)$$

where β_1 represents the propagation constant of TE_{10}, and β_2 represents the propagation constant of TE_{01}. By adjusting the

dimensions of the pyramidal horn (including the length, width and height of the waveguide transition), a shift of $90°$ is obtained for the relative phase between the two modes. As mentioned above, the $45°$-right inclined slot convert the excitation into two orthogonal modes of equal amplitude and $90°$ out of phase is produced by adjusting the dimensions of the pyramidal horn, thus excellent Right Hand CP (RHCP) is achieved. The RHCP is generated by the $45°$-right inclined slot. On the contrary, if the modal has a $45°$-left inclined slot (also form top view), then Left Hand CP can be achieved.
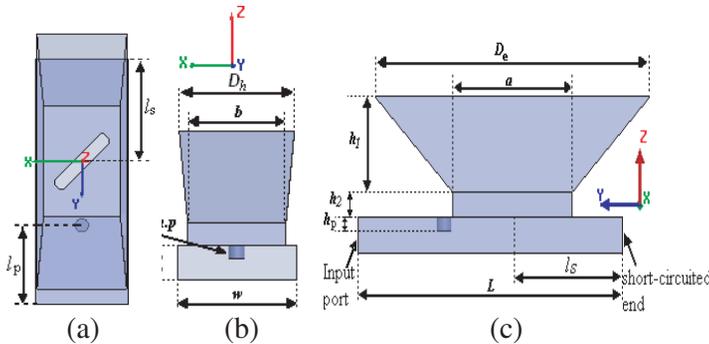
Figure 2. The dimensions of the horn antenna. (a) Top view of horn antenna for the location of the inclined slot and the pin. (b) Front view in terms of the dimensions of the rectangular waveguide. (c) Side view in terms of the dimensions of the horn antenna.

The classical theory approaches [17] is used to analyze the radiation characteristics of the pyramidal horn and to verify the feasibility of the horn element design. Assume that the phase distribution on the mouth of pyramidal horn changes along the X and Y direction in the way of uniform square rate. Pyramidal horn is excited by TE_{10} and TE_{01}, and its total aperture field is shown in formula (3):

$$\begin{cases} \mathbf{E}s = \hat{y}E_y^{10} + \hat{x}jE_x^{01} \\ \mathbf{H}s = -\hat{x}E_y^{10}/\eta + \hat{y}jE_x^{01}/\eta \end{cases} \tag{3}$$

where $\eta = 120\pi$ is the free-space wave impedance, E_y^{10} the electric field of the TE_{10} mode, E_x^{01} the electric field of the TE_{01}, and formulas of these two field components can be referenced to the literature [17]. The complex number j is phase difference of the two field components, equal to $\pi/2$.

The far field E_θ and E_φ can be shown in (4) by vector wave

functions:

$$\begin{cases} E_\theta = -\mathrm{j}\frac{e^{-\mathrm{j}\beta r}}{2\lambda r}(L_\varphi + \eta N_\theta) \\ E_\varphi = \mathrm{j}\frac{e^{-\mathrm{j}\beta r}}{2\lambda r}(L_\varphi - \eta N_\theta) \end{cases}. \tag{4}$$

where the vector wave functions of L_φ and N_θ can be referenced to the literature [18]. λ is the wavelength and β the propagation constant. Based on the above theoretical analysis and combined with the calculation and simulation, a horn element has be designed. The dimensions of the mechanical design are shown in Fig. 2.

The main design parameters determining the electromagnetic characteristics of the antenna are as follows: D_e is the length of the aperture of the horn, D_h the width of the horn, h_1 the height of the horn, and a, b and h_2 are the length, width and height of the waveguide transition, respectively. w is the width of the rectangular waveguide, h_3 the height of the rectangular waveguide, l_s the distance from the center of the slot to the short-circuited end of rectangular waveguide, and l_p the distance from the center of the pin to the input port. The rectangular waveguide length (L) is not critical, as long as it extends beyond the length for the attenuation of undesired modes, as shown in Table 1.

Table 1. The detail dimension of the element in wavelength.

Parameter	Value	Parameter	Value
D_e	1.845	D_h	0.6548
a	0.7976	b	0.5595
w	0.6774	$h3$	0.1786
l_s	0.7381	l_p	0.5738
h_p	0.07143	Diam. of pin	0.09524
h_1	0.4762	h_2	0.1190
Width of Slot	0.09405	Length of Slot	0.5119
L	1.771		

2.2. Simulation of Element

To determine the parameter values of the design, we perform optimization of the horn antenna using Ansoft HFSS. According to the simulation in Ansoft HFSS, the final design parameters of the antenna are determined as shown in Table 1.

The radiation patterns and reflection coefficient are shown in Fig. 3. Aluminium is used as the material for all the metallic parts. All the dimensions are internal to the horn antenna, in order to make them independent of the metal's thickness. The simulated reflection coefficient of the rectangular waveguide port is shown in Fig. 3(a) in 0.01 fc-bandwidth at Ka-band, and fc represents the center frequency. The element has a maximum reflection coefficient of −20 dB. However, the reflection coefficient increases sharply to −13 dB without loading the pin. Therefore, the pin along the rectangular waveguide is essential to the impedance matching. Fig. 3(b) shows the simulated RHCP radiation pattern and the cross-polarization (LHCP) for two orthogonal planes, the azimuth plane and the elevation
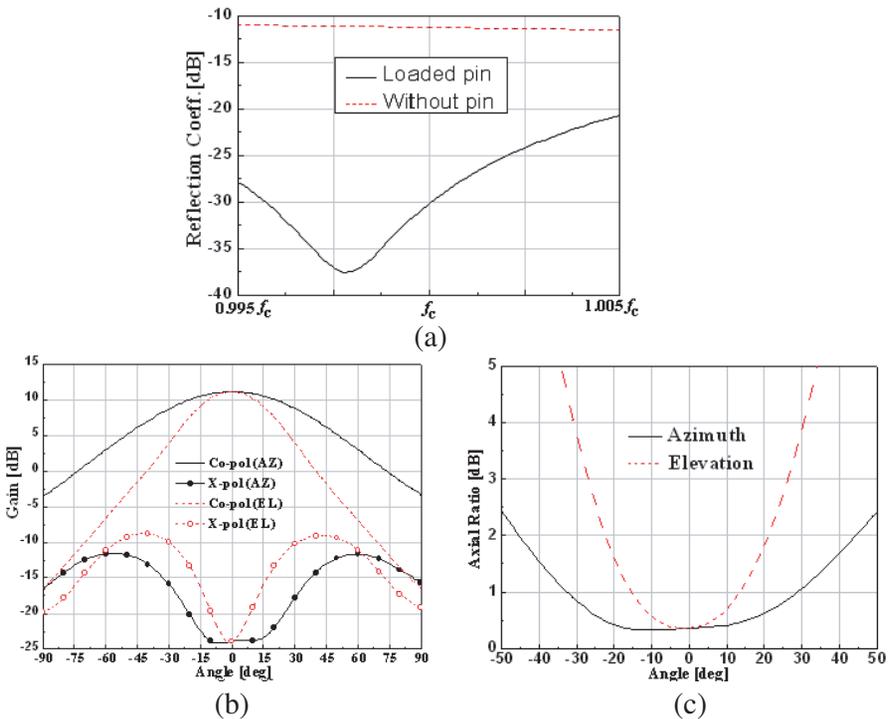
Figure 3. Simulated results of element antenna: (a) The reflection coefficients at the rectangular waveguide port for Ka-band. (b) The simulated RHCP (Co-pol) gain and LHCP (X-pol.) gain, the 'AZ' is abbreviation for Azimuth plane and the 'EL' is abbreviation for Elevation plane. (c) The simulated axial ratio for the azimuth and elevation planes of the element.

plane. Excellent symmetry and good cross polarization rejection can be observed. The element antenna has gain of 11 dBi at center frequency fc, and the -3 dB beamwidth is approximately $38°$ in the elevation plane and more than $60°$ in the azimuth plane. Fig. 3(c) depicts the element axial ratio for the -6 dB beamwidth in azimuth plane and elevation plane at center frequency fc. As common to other similar antennas, the axial ratio starts to degrade when the scanning angle is increased. However, axial ratio $< 3d$ over the main lobe beanwidth is achieved both in the azimuth and elevation planes.

3. ARRAY AND POWER DIVIDER NETWORK DESIGN

To produce monopulse Σ and Δ patterns and enhance the gain in the azimuth plane, an array design by using the horn antenna as element is described here. If the array is fed by two ports with in-phase or out-of-phase, monopulse Σ and Δ patterns, respectively, can be synthesized in one direction [19]. Therefore, a design for power divider network is also presented in this section.

3.1. Array Structure Design

To synthesize monopulse Σ and Δ patterns in the azimuth plane, a linear array is arranged along the X-axis. In order to design the array, the total number and the space of array elements should first be selected. In this design, the minimum number of antenna elements in the linear array is 28, as determined in the desired radiation patterns, and the most suitable element spacing (d) can be considered to be 0.88λ, λ is the wavelength at the center frequency. The left half of antenna array is shown in Fig. 4, and the right half is the same as the left.

Taking into consideration of sidelobe suppression, the linear array
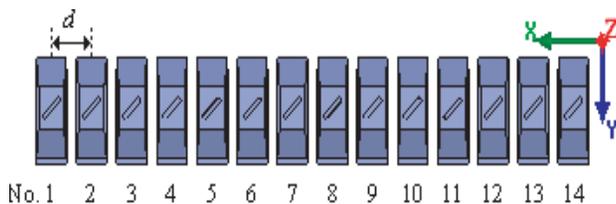
Figure 4. Left half of antenna array. d is element spacing. Since the right half of the array is same as the image of the left, the right half of array is not shown.

distributions are obtained via the use of the Taylor distribution. The left half of array normalized power distributions is given in Table 2, and the right half of the distribution is a mirror value of the left. For the azimuth pattern, a low sidelobe (-30 dB) Taylor distribution is achieved by using Taylor Synthesis Method to shape the main beam to the desired beam characteristics. On the other hand, for the elevation pattern, the radiation pattern characteristics of the element are still maintained.

Table 2. The left half of array normalized power distributions.

No. of element	Amplitude (dB)	No. of element	Amplitude (dB)
1	-11.95	8	-3.025
2	-11.21	9	-2.135
3	-9.944	10	-1.416
4	-8.413	11	-0.8529
5	-6.847	12	-0.4292
6	-5.388	13	-0.1435
7	-4.106	14	0

3.2. Power Divider Network Design

The power divider feed network has been designed to provide output amplitudes and phases exactly as required by the antenna array. The antennas for practical application are restricted in their structure due to mechanical scanning limitations. In such situations, the waveguide power divider network is a suitable building block for this antenna array [20], and this literature uses the four-port equivalent magic tee waveguide as the splitter, but we employ the there-port H-T waveguide as the splitter, and magic tee acts as a directional coupler and a phase shifter formed compact topological structure to design the power divider network. It is worth mentioning that the power divider network in this paper has the advantage of more precise machining. Fig. 5 shows the left half of topological structure of the $1:28$ power divider network, and there are 26 splitters in the entire power divider. The calculated power split ratios of 13 splitters in Fig. 5 are shown in Table 3.

The most critical component in this power divider for antenna array is the 3-port H-plane T (H-T) splitter [21]: It has to be designed precisely for various split ratios in order that the power divider network produces the amplitude and phase required for the array distribution
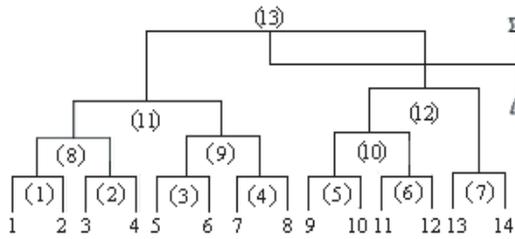
Figure 5. Left half of topological structure of the $1:28$ power divider network. The right half is a mirror image of the left. There are 13 splitters in the left of power divider.

Table 3. The caculated power split ratio of each splitters.

No. of splitter	Power split ratio (dB)	No. of splitter	Power split ratio (dB)
(1)	0.7341	(2)	1.5305
(3)	1.4586	(4)	1.0810
(5)	0.7188	(6)	0.4237
(7)	0.1435	(8)	2.4536
(9)	2.5243	(10)	1.1245
(11)	5.5540	(12)	−1.9196
(13)	4.5407		

function. The VSWR at the central port (P1) of the H-T junction must be kept very low because the feed network cannot tolerate impedance mismatch.

In addition, to realize the constant phase of array excitation, the effective path length differences between the H-T splitter output ports has to be taken into account. The splitter is shown in Fig. 6, and it allows us to alter the power split ratio P3/P2 and VSWR at port 1 by changing the position (x) and length (L) of a septum and the width (w) of the iris.

To reduce the width of the power divider network, mitered waveguide bends and slot-coupling have been utilized in this design. Based on the topological structure which is shown in Fig. 5, the configuration of power divider is presented in Fig. 7. But splitters from No. 1 to No. 7 are folded and fed through the slots to reduce the width of the power divider network. In Fig. 7(b), from the front view,
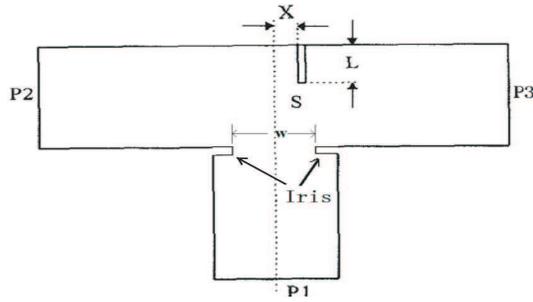
Figure 6. Reactive H-T splitter geometry.
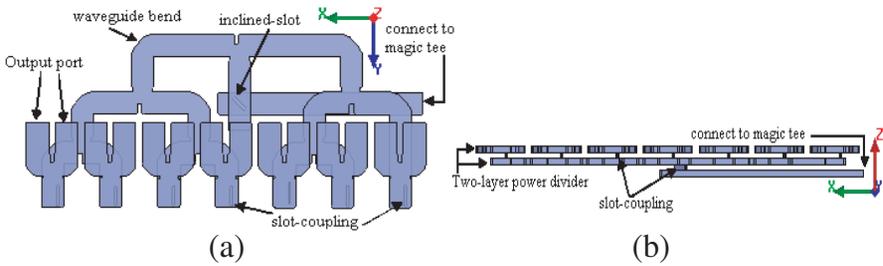
Figure 7. Configuration of the left half of waveguide power divider. (a) Top view of the power divider. (b) Front view of the power divider.

the waveguide power divider has two layers. Splitters from No. 1 to No. 7 are arranged in the upper layer and other splitters positioned in the lower layer. The electromagnetic wave is coupled form lower layer to upper layer through slots. Based on the dimensions of slot mentioned in Table 1, all lengths of these slots vary in certain scope to be resonance slots for transferring maximum energy from the lower layer to upper layer.

Magic tee acts as a directional coupler and a phase shifter. In this design, the magic tee can be obtained by slot-coupling combination of two parts. Fig. 8 shows the structure of the magic tee. From the front view, the upper layer is the feed path of the Σ port, which directly connects to the power dividers. The lower layer is the feed path of the Δ port and feeds the power dividers through the coupling slot. In addition, the position of the pin in the waveguide of the Σ port can be adjusted for the best impedance matching.

The magic tee and power dividers are connected to build a compact monopulse combining network. Its configuration is shown in Fig. 9. Since the power divider network has a complicated structure
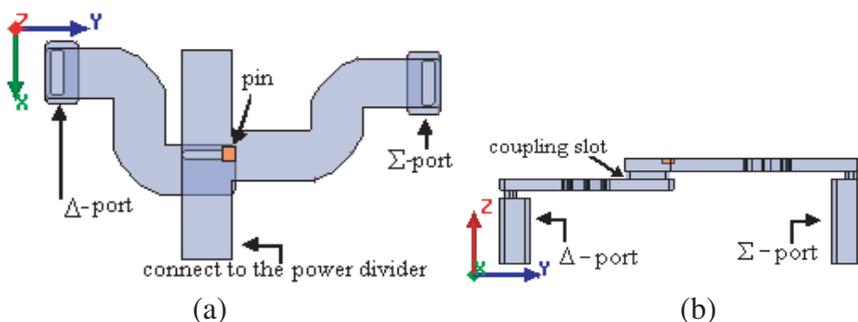
Figure 8. Configuration of the magic tee. (a) Top view. (b) Front view.
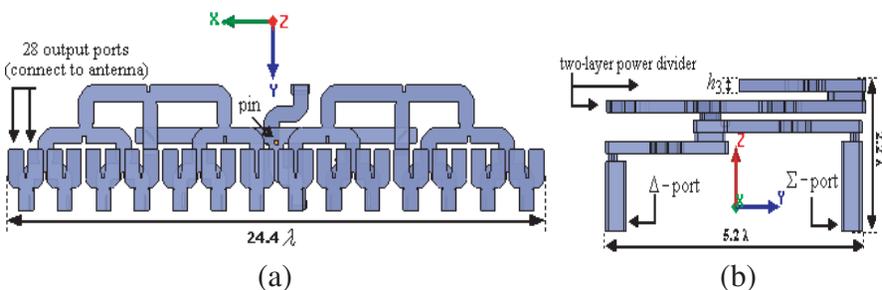
Figure 9. Configuration of the power divider network. (a) Top view of the power divider network. (b) Front view of the power divider network.
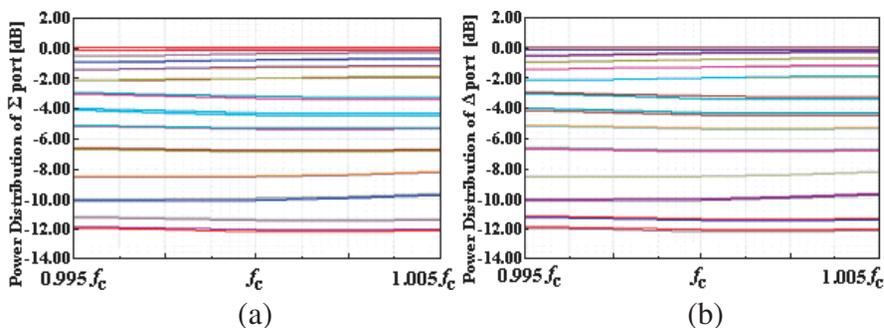
Figure 10. Power distribution of the power divider feed network. (a) Power distribution of 28 elements when excited at Σ port. (b) Power distribution of 28 elements when excited at Δ port.
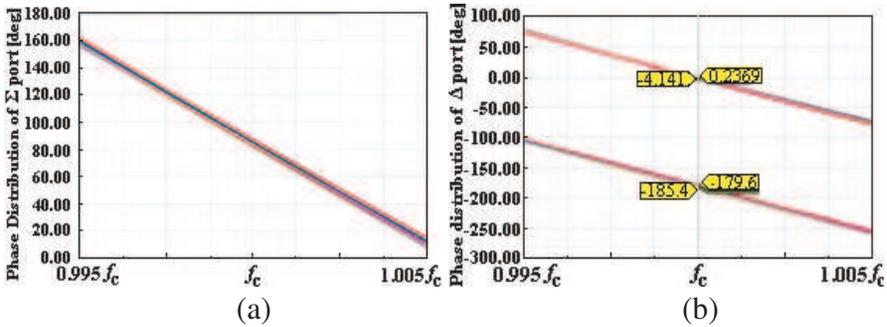
Figure 11. Phase distribution of the power divider feed network. (a) Phase distributions of 28 elements when excited at Σ port. (b) Phase distribution of 28 elements when excited at Δ port.

for synthesizing monopulse Σ and Δ patterns in the azimuth plane, it is difficult to list all detailed dimensions of the structure. The dimensions of the entire power divider network are expressed by λ, and the height of each layer's waveguide is $h3$ the same as the height of the element's rectangular waveguide.

The simulated dividing characteristics are presented in Fig. 10 and Fig. 11. As shown in Fig. 10(a) and Fig. 10(b), the simulated amplitudes at the 28 output ports deviate by up to ± 0.3 dB compared with the calculated results given in Table 2. Fig. 11(a) shows the maximum phase discrepancy over all ports is up to ± 3 degrees when the power divider network is excited at Σ port. In Fig. 11(b), the relative phase between the left half 14 output ports and right half 14 output ports is approximately $180°$ out-of-phase when the Δ port is used. Since the power divider network has a compact structure, it cannot neglect the influence of discontinuity (including septum, iris and coupling-slots even for the very narrow bend-to-bend or bend-to-splitter spacing and so forth) encountered in the present power divider network, and the simulated values shift a little compared with the theoretical prediction. However, the results of power divider network are still desirable.

Simulated results of VSWR of the two ports are shown in Fig. 12(a). The power divider network has maximum VSWR of 1.14 for Σ port and 1.10 for Δ port across the operating bandwidth. Fig. 12(b) shows the isolation characteristic of two ports, and the minimum isolation is approximately 31.5 dB over the working bandwidth.

In order to achieve accuracy in the simulation of the network, each splitter needs to be designed carefully in the 0.5 degrees and 0.2 dB range for the phase balance and amplitude match before making up the
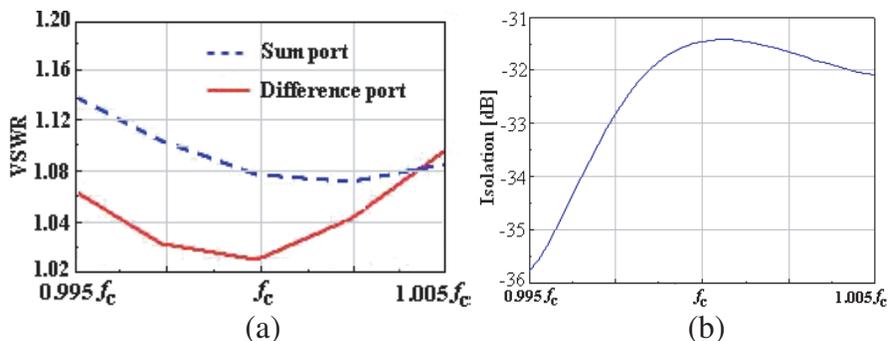
Figure 12. Simulated results of the two ports. (a) VSWR of the two ports. (b) Isolation between the two ports.

feeding network. In addition, the feed network simulation also needs to take into account the electrical path length of the power divider H-T junctions as well as of the bends, coupling slots and straight line sections, which are vital to the output ports' phase of the power divider network.

4. MEASURED AND SIMULATED RESULTS

A 28-element linear array model with power divider network described in the previous section is presented in Fig. 13(a). This model is used for detailed simulation analysis of the entire array's characteristics. The fabricated array prototype is shown in Fig. 13(b). As shown in Fig. 13(c), the fabricated array consists of six-layer aluminium plates, and each aluminium plate is the relative part as follows: (1) pyramidal horn array; (2) rectangular waveguide and the upper layer of power divider network; (3) the lower layer of power divider network; (4) the feed path of Σ-port; (5) the feed path of Δ-port; (6) two waveguide of two ports. These layers must be tightly assembled by welding. The welding quality and the fabrication error can adversely affect the radiation characteristics and impedance matching of the array.

Figure 14 illustrates a good agreement between the measured and simulated reflection coefficients at two ports covering the required bandwidth under the criterion of less than -15 dB. Fig. 16 shows the measured and simulated monopulse normalized patterns in the azimuth plane at the center frequency. The agreement between the simulated and measured values in the Σ pattern supports the technical feasibility in the previous design. In the Δ pattern, since the fabricated power divider network must take into account the errors of processing, the
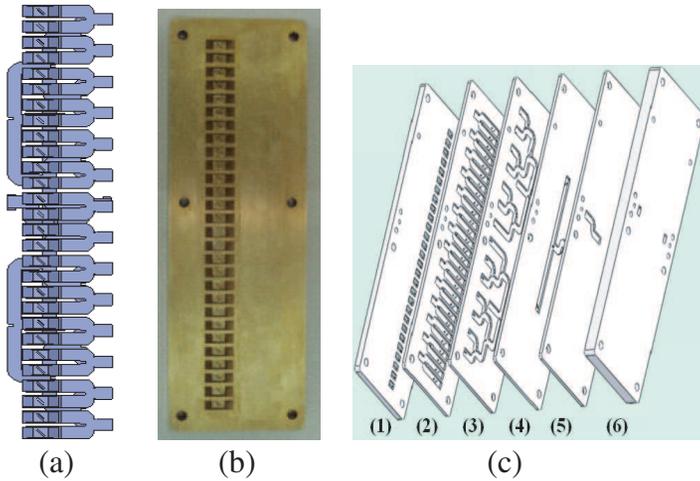
Figure 13. Structure of the array with power divider network. (a) Configuration of the simulated model. (b) Fabricated array prototype. (c) Details for the fabricated array in each layer.
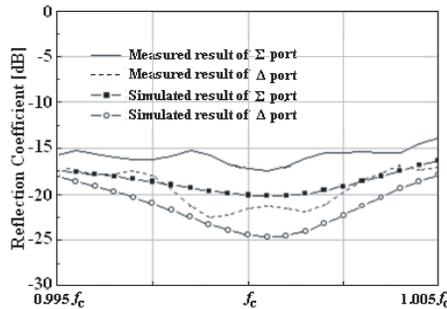
Figure 14. Simulated and measured reflection coefficient at Σ-port and Δ-port.

measured value of null depth is less than 30 dBi while the simulated value of null depth is more than 31 dBi.

As shown in Fig. 15(b), there exists a moderate difference between the radiation patterns from the measurement and simulation in the elevation plane. Both the measured and simulated -3 dB beamwidth in elevation plane are approximately $38°$ when the array is excited at the Δ port. At scanning angle of $0°$, the measured Σ/Δ ratio is approximately 26 dB, while the simulated Σ/Δ ratio is more than 31 dB. These values of Σ/Δ ratio accord with the values of null-depth

in azimuth plane. However, the radiation patterns are not symmetrical in the elevation plane, especially when the array is excited at the Δ port. The result is caused by the asymmetric structure of array in the elevation plane.

In Table 4, the main values of the array in both the simulated and

Table 4. Summary of comparison in two planesat three frequencies.

Parameters		0.995 fc	fc	1.005 fc
−3 dB beam-width	Simulate	2.8°	2.8°	2.8°
in azimuth	Measure	2.7°	2.6°	2.5°
−3 dB beam-width	Simulate	38.3°	38.3°	38.3°
in elevation	Measure	37.9°	38.1°	37.2°
SLL	Simulate	−27.3	−28.9	−28.6
(dB)	Measure	−28.2	−28.5	−28.5
Null depth	Simulate	−33	−31.6	−31
(dB)	Measure	−28.1	−26.2	−30.5
The level difference	Simulate	0.06	0.03	0.05
of Δ beam (dB)	Measure	0.37	0.52	0.13

(a)   (b)
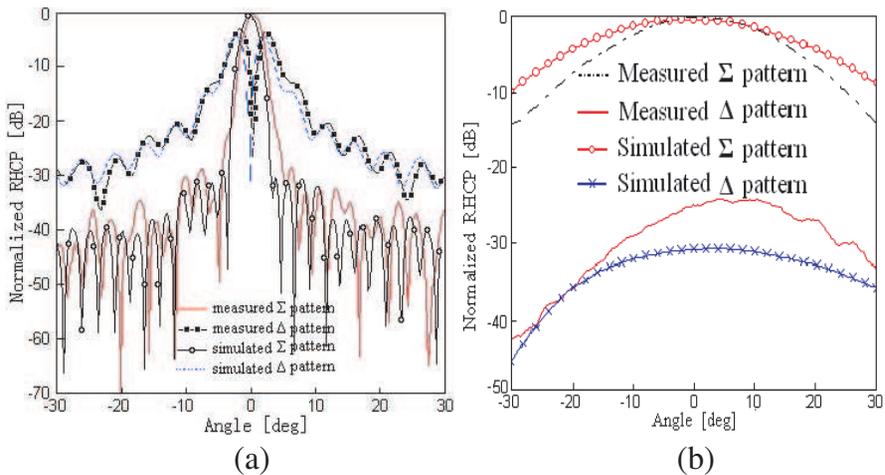
Figure 15. (a) Simulated and measured Σ and Δ patterns of azimuth plane in center frequency. (b) Simulated and measured Σ and Δ patterns of elevation plane in center frequency.

measured results at three different frequencies in two main planes are summarized for easy comparison. The values of SLL are below -27 dB at three frequencies. The Δ patterns also indicate good symmetry with a less than -26 dB deep null on-axis at three frequencies. Note that the values of level difference and null-depth in measurement are worse than that in simulation. The cause of the difference is due to superposition effects of residual mismatches at the ports' waveguide loads and the errors relevant to actual machining process conditions. Fig. 16 illustrates the axial ratio of array for the -3 dB beamwidth in two planes at the center frequency. Both the measured and simulated axial ratio are lower than 3 dB, showing good circularity of the array.
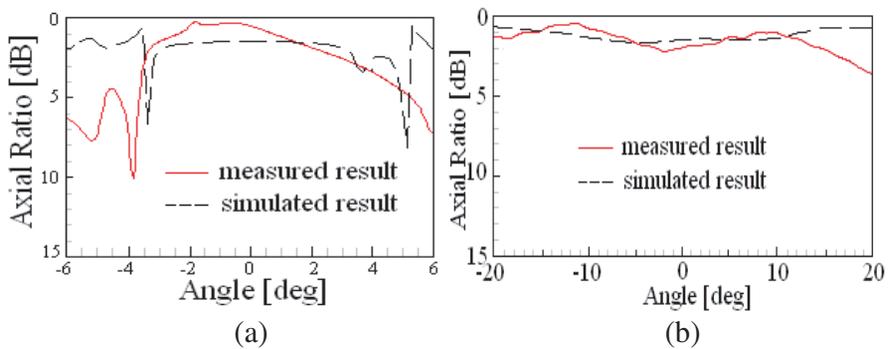
Figure 16. Simulated and measured axial ratio of array antenna for -3 dB beamwidth in two main planes at center frequency. (a) Axial ratio in the azimuth plane (approx. $\pm 3°$). (b) Axial ratio in the elevation plane.(approx. $\pm 40°$).

5. CONCLUSION

In this paper, a novel and compact feed structure in a rectangular waveguide is proposed to achieve RHCP. The $45°$-right inclined slot convert the excitation into two orthogonal modes of equal amplitude and $90°$ out of phase is produced by adjusting the dimensions of the pyramidal horn. Compared to ordinary CP horn antenna, the proposed antenna has a compact structure without polarizer, and the element can be easily fabricated owing to its structural characteristics.

By means of the presented novel design of power divider network, the monopulse pattern synthesis has been made. A prototype antenna array is fabricated, and the radiation characteristics are measured. The agreement between the measurement and simulation verifies the capability of the circularly polarized array for the monopulse tracking operation. In addition, although there are many slots, septa, irises

and pins loaded in the power divider network, which will lead to complicated structure, 90% fabricated arrays have almost the same characteristics as described in our paper. This high yield supports the technical feasibility of the design.

REFERENCES

1. Bullock, L. G., G. R. Oeh, and J. J. Sparagna, "An analysis of wide-band microwave monopulse direction finding techniques," *IEEE Transactions on Aerospace and Electronic Systems*, Vol. 7, No. 1, 188-203, Jan. 1971.

2. Strauss, G. and K. Breitsameter, "A circular polarized tem horn antenna array with large scanning angle," *2011 IEEE Radio and Wireless Symposium*, 98–101, Jan. 2011.

3. Gan, T. H. and E. L. Tan, "Design of waveguide fed broadband circular polarization truncated horn antenna for high power applications," *2011 Asia-Pacific Microwave Conference Proceedings*, 1194–1197, Dec. 2011.

4. Du Toit, J. B., D. E. Baker, and A. J. Booysen, "Design and development of an 8 to 12 GHz circularly polarized two element horn antenna array with high isolation," *2012 IEEE-APS Topical Conference on Antennas and Propagation in Wireless Communications*, 1005–1008, Sep. 2012.

5. Franco, M. J., "A high-performance dual-mode feed horn for parabolic reflectors with a stepped-septum polarizer in a circular waveguide," *IEEE Antennas and Propagation Magazine*, Vol. 53, No. 3, 142–146, Jun. 2011.

6. Chen, M. and G. Tsandoulas, "A wide-band square-waveguide array polarizer," *IEEE Transactions on Antennas and Propagation*, Vol. 21, No. 3, 389–391, May 1973.

7. Bornemann, J. and S. Amari, "Septum polarizer design for antenna feeds produced by casting," *IEEE International Symposium on Antennas and Propagation Digest*, No. 2, 1422–1425, Montreal, Jul. 1997.

8. Behe, R. and P. Brachat, "Compact duplexer-polarizer with semicircular waveguide," *IEEE Transactions on Antennas and Propagation*, Vol. 39, No. 8, 1222–1224, Aug. 1991.

9. Hazdra, P., R. Galuscak, and M. Mazanek, "Optimization of prime-focus circular waveguide feed with septum polarization transformer for 1.296 GHz EME station," *Proceedings of the First European Conference on Antennas and Propagation*, Nice, Nov. 2006.

10. Leal-Sevillano, C. A., J. R. Montejo-Garai, J. M. Rebollar, and J. A. Ruiz-Cruz, "CAD for dual-band polarizers in corrugated rectangular waveguide," *2011 41st European Microwave Conference*, 822–825, Oct. 10–13, 2011.

11. Yun, J., S. Jeon, and J. Chae, "Feed horn antenna including circular-polarizer and straight type mode converter to illuminate shaped reflector at Ka-band," *2004 IEEE Antennas and Propagation Society International Symposium*, 1559–1562, 2004.

12. Tucholke, U., F. Arndt, and T. W. Riedt, "Field theory design of square waveguide iris polarizers," *IEEE Transactions on Microwave Theory Technology*, Vol. 34, No. 1, 156–160, Jan. 1986

13. Yoneda, N., R. Miyazaki, I. Matsumura, and M. Yamato, "A design of novel grooved circular waveguide polarizers," *IEEE Transactions on Microwave Theory Technology*, Vol. 48, No. 12, 2446–2452, Dec. 2000.

14. Lee, C. S., S. L. Chuang, and S. W. Lee, "A simple version of corrugated guide: Smooth-walled circular waveguide coated with lossy magnetic material," *Antennas Propagation Soc. Int. Symp. Dig.*, Vol. 1, 303–306, 1985.

15. Lee, C. S., S.-W. Lee, and D. W. Justice, "A simple circular-polarized antenna: Circular waveguide horn coated with lossy magnetic material," *IEEE Transactions on Antennas and Propagation*, Vol. 36, No. 2, 297–300, Feb. 1988.

16. Pozar, D. M., *Microwave Engineering,* 4th Edition, John Willey & Sons, Inc., 2011.

17. Balanis, C. A., *Antenna Theory: Analysis and Design*, 3rd Edition, John Willey & Sons, Inc., 2005.

18. Balanis, C. A., *Advanced Engineering Electromagnetics*, Wiley, 1998.

19. Miyashita, H. and T. Katagi, "Radial line planar monopulse antenna," *IEEE Transactions on Antennas and Propagation*, Vol. 44, No. 8, 1158–1165, Aug. 1996.

20. Varghese, J., M. S. Easwaran, S. Christopher, and Y. M. Rao, "Computer aided design of planar waveguide monopulse comparator for low height airborne antennas," *Proc. Radar. 97, Electron and Radar. Conference*, 522–525, Oct. 1997.

21. Arnold, E., R. W. Lyon, A. Schlaud, K. Solbach, and J. S. Tanner, "Design of a power divider network for a slotted waveguide array using finite element and finite difference techniques," *Eighth International Conference on Publication Antennas and Propagation*, Vol. 2, 831–833, 1993.